Grundmann, G., Förster, H.-J. (2018): The Sierra de Cacheuta Vein-Type Se Mineralization, Mendoza Province, Argentina. - *Minerals*, *8*.

DOI: http://doi.org/10.3390/min8040127

minerals

MDPI

Article

The Sierra de Cacheuta Vein-Type Se Mineralization, Mendoza Province, Argentina

Günter Grundmann [1] and Hans-Jürgen Förster [2,*]

[1] Eschenweg 6, DE-32760 Detmold, Germany; grundmann.g@gmx.de
[2] Helmholtz Centre Potsdam German Research Centre for Geosciences GFZ, DE-14473 Potsdam, Germany
* Correspondence: forhj@gfz-potsdam.de; Tel.: +49-0331-288-28843

Received: 14 February 2018; Accepted: 15 March 2018; Published: 22 March 2018

Abstract: The Sierra de Cacheuta vein-type Se mineralization in the Mendoza Province predominantly consists of clausthalite, klockmannite, eskebornite, eucairite, and naumannite. These primary selenides formed in a fault zone, cutting through fine-grained trachytic host rock. Cross-sections perpendicular to the veinlets, polarized light microscopy, and scanning-electron microscopy, combined with electron-microprobe analysis, provide a record of the relationship between different crystallization and deformation events. Mineralization encompasses four episodes of fault formation (*d*1–*d*4): early zonal selenide crystallization (stage (**I**)); ductile deformation of the selenides (stage (**II**)); fault re-opening, fluid-mediated metal mobilization, metalliferous-fluid infiltration, and mineral precipitation (stage (**III**)); and subsequent alteration (stage (**IV**)). The Se vein originated from multiple injections of highly oxidized, metal-rich fluids. These low-T solutions (estimated max. temperature 100 °C, max. pressure 1 bar) possessed high to exceptionally high Se fugacities (log f_{Se2} between −14.5 and −11.2) that prevailed for most of the evolution of the deposit. The source of the Se and the accompanying metals (Cu, Ag, Pb, and Fe) is probably the neighboring bituminous shale. The deposition of Se minerals occurred when the oxidized metal-bearing solutions came in contact with a reductant, which caused the reduction of mobile selenate to immobile selenide or elemental Se. We identified several features that permit us to safely distinguish samples from Cacheuta from Argentinian Se deposits in the Province of La Rioja: (I) trachytic host rock fragments containing bitumen and TiO_2 pseudomorphs after titanomagnetite; (II) early Co-rich and Ni-poor krut'aite (Co < 6.7 wt %, Ni < 1.2 wt %) partly replaced by clausthalite, umangite, klockmannite, eskebornite, Ni-poor tyrrellite (Ni < 2.7 wt %), Ni-poor trogtalite (Ni < 1.2 wt %), and end-member krut'aite and petříčekite; (III) lack of calcite gangue; and (VI) Se-bearing alteration minerals comprising chalcomenite, molybdomenite, cobaltomenite, an unnamed Cu selenide (for which the ideal formula may be either Cu_2Se_3 or Cu_5Se_8), and possibly mandarinoite, mereheadite, orlandiite, and scotlandite as new species for this occurrence.

Keywords: selenium mineralization; trachytic host rock; tyrrellite; trogtalite; krut'aite; petříčekite; genetic sequence; Sierra de Cacheuta; Argentina

1. Introduction and Geological-Historical Background

In the South American Andes, the provinces of La Rioja and Mendoza in Argentina host several mineralogically important selenium occurrences [1]. Modern research on Argentinian selenium deposits has mainly focused on the study of rare or new Se species, the determination of their chemical composition, and the definition of their crystal structure [2–7]. Minor effort has been spent studying in detail the origin of the various selenide occurrences, notably the relationship between the crystallization and deformation of the selenium mineralization and its host rock. This particularly holds true for the selenium mineralization in the Sierra de Cacheuta district, also known as el Cerro de Cacheuta,

in the Mendoza Province. Sierra de Cacheuta is the type locality of achavalite FeSe, chalcomenite $CuSeO_3 \cdot 2H_2O$, cobaltomenite $CoSeO_3 \cdot 2H_2O$, and molybdomenite $PbSeO_3$.

Nowadays, the location of the Sierra de Cacheuta Se occurrence is not precisely known; it has never been recovered [1,8]. It was discovered sometime between 1860–1862 [9]. In the earliest and most detailed description of the area, the following information was provided [10]: The occurrence encompasses several small selenide veinlets ranging in thickness from 1–2 mm to a maximum of 4 cm. The main selenium minerals were clausthalite and copper selenides. Near the surface, the ore veins contained Ag contents of up to 21 wt %. At depth, the Ag content decreased rapidly down to almost zero at only 12 m depth—the reason why the mining activity had been terminated.

Geographically, the occurrence was located on the right bank of the Rio de Mendoza, where it came from the Sierra de Cacheuta in the West [9,10]. The mines were on the southern slope of the mountain range, a few leguas (miles) from the river. The slope was built up by andesitic to trachytic rocks, which had vesicular cavities locally filled with calcite or agate. The volcanic host rocks varied in texture from stratified to massive and were irregularly jointed. Stelzner examined the post-volcanic selenium veinlets in several small galleries, which were mined at different heights on the slope. On the surrounding dumps, he found only two little veinlet fragments, consisting mainly of granular ankerite and minor ore minerals. At the bottom of the mountain range, sandy, calcareous, or marly sediments occurred, with intercalations of bituminous shale and local asphalt enrichment. Brackebusch (1893) [11] also mentioned bitumen ("Erdpech" in German) as a constituent of the Se veins. Ramdohr (1975) [12] identified the following main ore minerals: klockmannite, clausthalite, eukairite, umangite, naumannite, accessory ferroselite, and two unspecified cobalt selenides. The sulfides were chalcopyrite and pyrite.

The first black and white photomicrographs and mineral reflectance and compositional data, as well as a crystallization sequence of selected selenides from Cacheuta, were erroneously published under the locality name "Los Llantenes, La Rioja, Argentina" [2]. This mistake was later noted by [1], who also provided new color photomicrographs and mineral-chemical data for the same sample (No. #49). Confusion regarding the Argentinian Se occurrences may be frequent, considering that even the newest online encyclopedias (e.g., mindat.org; Mineralienatlas; Wikipedia) and books bear inconsistencies in terms of the mineral content, macrostructure, microstructure, and chemical composition for the individual Se occurrences.

Our examination of 16 polished sections prepared from 11 "historic" Se-vein fragments (Collection F.N. Keutsch, Harvard University, Cambridge, MA, USA; labeled as "Cacheuta", or "Cerro de Cacheuta", or "Sierra de Cacheuta") permits us to elaborate upon a comprehensive paragenetic scheme for this mineralization. Application of special sample preparation techniques permitted an in-depth study of the internal structure of the different types of Se-veinlets discriminated at Cacheuta. We report new microstructural and chemical data for the selenium vein mineralization, also addressing its host rock. We provide a genetic model that considers the relationship between the crystallization and deformation of the primary and secondary minerals, and we discuss possible mechanisms for the formation of that unique Se occurrence. Finally, we discuss diagnostic features that allow us unequivocally to distinguish samples from Cacheuta from those of the Se occurrences in the Province of La Rioja in Argentina.

2. Methods

Petrographic and microstructural studies were mainly performed by optical microscopy (Leitz DMRM polarizing microscope, Type 301-371-010, Leitz/Leica, Wetzlar, Germany). Information on microstructure was obtained from Se-vein fragments cut and polished perpendicular to the vein wall and selvages. Sample preparation involved the following machinery and materials: lapping and polishing machine type "Buehler Metaserv", Buehler UK Ltd., Coventry, UK; grinding and polishing machine type "Kent MK 2A", Engis Ltd., UK; "Pellon" polishing chemotextile type PAN-W, Hartfeld & Co., Allerod, Denmark; diamond suspension, water soluble (grain sizes 6 μm, 3 μm, 1 μm, 0.25 μm)

type Gala-Tec GmbH, Kaiserslautern, Germany; SiC grinding powder (600, 800, 1000, 1200 mesh), fixed abrasives are steel discs, consisting of diamond in steel-binding (grain sizes 600, 800, 1200 mesh). For the surface treatment of the vein sections, two different preparation methods were used:

(a) Rolling grinding (loose abrasive grains). In this case, the surface is velvet. In dispersed-light dark field illumination, the internal structures (like foliation and fine folding) of the opaque metallic minerals are clearly visible.
(b) Polishing (bonded abrasive grains). In this case, the surface is polished. In dispersed-light dark field illumination, the polished opaque metallic minerals appear black.

Selenides and sulfides were routinely checked for concentrations of Cu, Ag, Pb, Hg, Fe, Co, Ni, Zn, As, Sb, Bi, S, and Se. Quantitative chemical analyses were conducted in WDS mode, using a JEOL electron probe X-ray microanalyzer JXA-8230 (JEOL, Akashima, Japan). The probe was operated at 20 kV, 20 nA; the beam size was 1–2 µm. The counting time on peak was 20 s, with half that time on background on both sites of the peak. The following standards, emission lines and analyzing crystals (in parentheses) were used (detection limits in ppm in brackets): Cu [200]—natural eskebornite, *Kα* (LIFL); Ag [300]—natural bohdanowiczite, *Lα* (PETJ); Pb [500]—natural clausthalite, *Mα* (PETH); Hg [800]—cinnabar, *Lα* (LIFL); Fe [150]—pyrite, *Kα* (LIFL); Co [180]—cobaltite, *Kα* (LIFL); Ni [200]—pentlandite, *Kα* (LIFL); As [300]—cobaltite, *Lα* (TAP); Sb [300]—InSb, *Lα* (PETJ), Bi [450]—synthetic Bi_2Se_3, *Mα* (PETH); S [100]—chalcopyrite, K*α* (PETJ); and Se [700]—natural naumannite, *Kα* (LIFL). The CITZAF routine in the JEOL software, which is based on the $\phi(\rho Z)$ method [13], was used for data processing. Selenates were studied by semi-quantitative EDS analysis using the same device.

3. Results

3.1. Petrography of Trachytic Host Rock

Lens-like trachytic host rock fragments of up to 2 cm in size are present inside the Se veinlets, forming a rubble breccia and/or boudinage (Figure 1). The altered fragments are generally stained greenish, bluish, reddish, and/or brownish by finely dispersed secondary minerals, such as malachite, celadonite, azurite, chalcomenite, hematite, and goethite (Figure 2a). The grain size of the fine-grained, non-oriented silicate matrix ranges between 0.1 and 2 mm. The groundmass shows an intersertal texture with twinned feldspar laths and interstices filled with greenish alteration products (celadonite pseudomorphs?) of pre-existing mafic phenocrysts (amphiboles).

Compression caused brittle deformation, producing a finely branched network of fractures and foliation planes throughout the matrix, occasionally forming lens-like or boudinaged fragments (Figure 1). Areas of the strongest foliation are stained greenish by malachite or brownish by goethite (Figure 2a). Optical polished-section analysis (Figure 2a,b) revealed the following modal mineralogy (estimated volume percentages in parentheses): feldspar (~85), clay (~10), celadonite (~4), and accessory components (~1), including reddish or yellowish pseudomorphs after titanomagnetite phenocrysts (average size 70 µm). These pseudomorphs consist of a framework of oriented leucoxene or hematite as alteration products, likely formed by oxidation of the original titanomagnetite containing oriented ilmenite laths. Single crystals and twinned or radially grown crystal aggregates of ferroselite were rare and confined to larger rock fragments (Figure 3). Irregular black patches of bitumen (up to a few millimeters) occurred as fracture fillings, cementing the host rock fragments from the vein wall inwards (Figure 4).

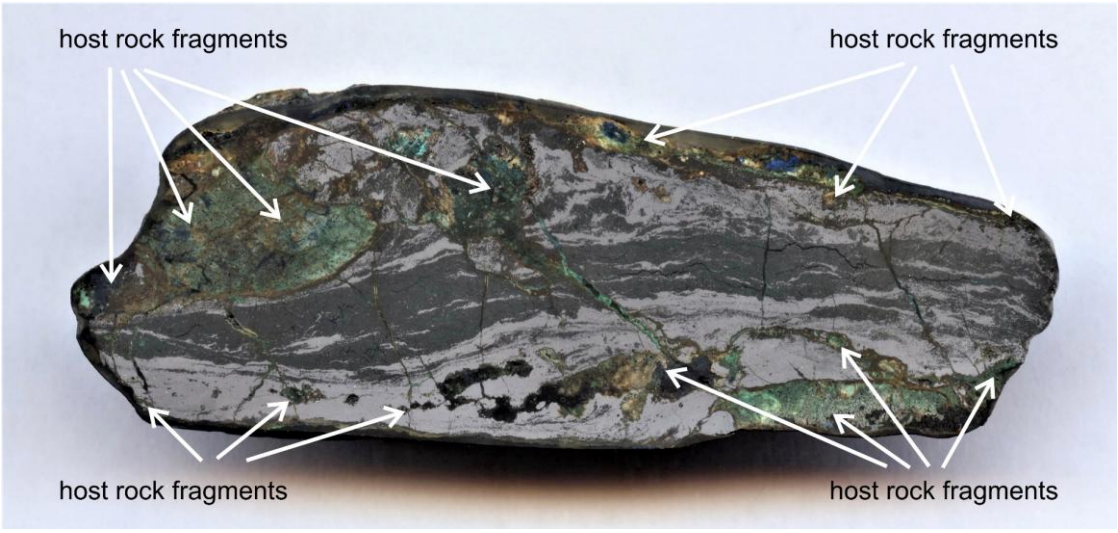

Figure 1. Dispersed-light dark field image of Se-vein Type-4 (2.2-cm-thick, 6.6-cm-wide, embedded in resin, surface rolling grinded, with 1.200 mesh SiC abrasive), with layers and lenses of klockmannite (dark grey) and clausthalite (light grey) forming a strongly foliated and folded mélange (cf. Section 3.2.1). The spotty and lens-like aggregates of the trachytic host rock fragments are partly rotated; the vein selvage, host rock fragments and diagonal fractures are stained by various alteration products, such as goethite (dark brown), azurite and chalcomenite (blue), and malachite (green).

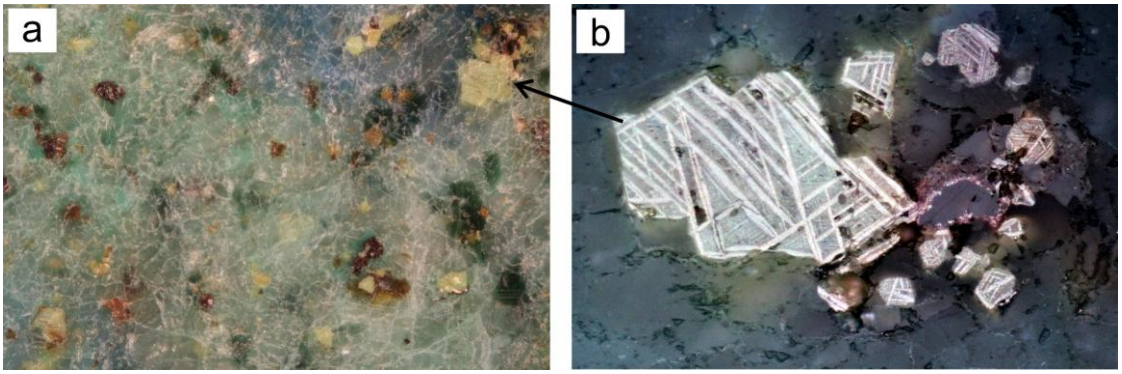

Figure 2. Details of a trachyte host rock fragment within a strongly foliated selenide veinlet (cf. Figure 1). (**a**) Interstices and heavily altered phenocrysts filled with greenish or bluish alteration products (malachite, azurite, or celadonite). Polished section, dispersed light dark-field image, width 2 mm. (**b**) Detail from Figure 2a (see black arrow) showing yellowish or brownish pseudomorphs consisting of a framework of oriented leucoxene lamellae originating in response to the alteration of titanomagnetite containing oriented ilmenite laths. Polished section, reflected light digital image, width 2 mm.

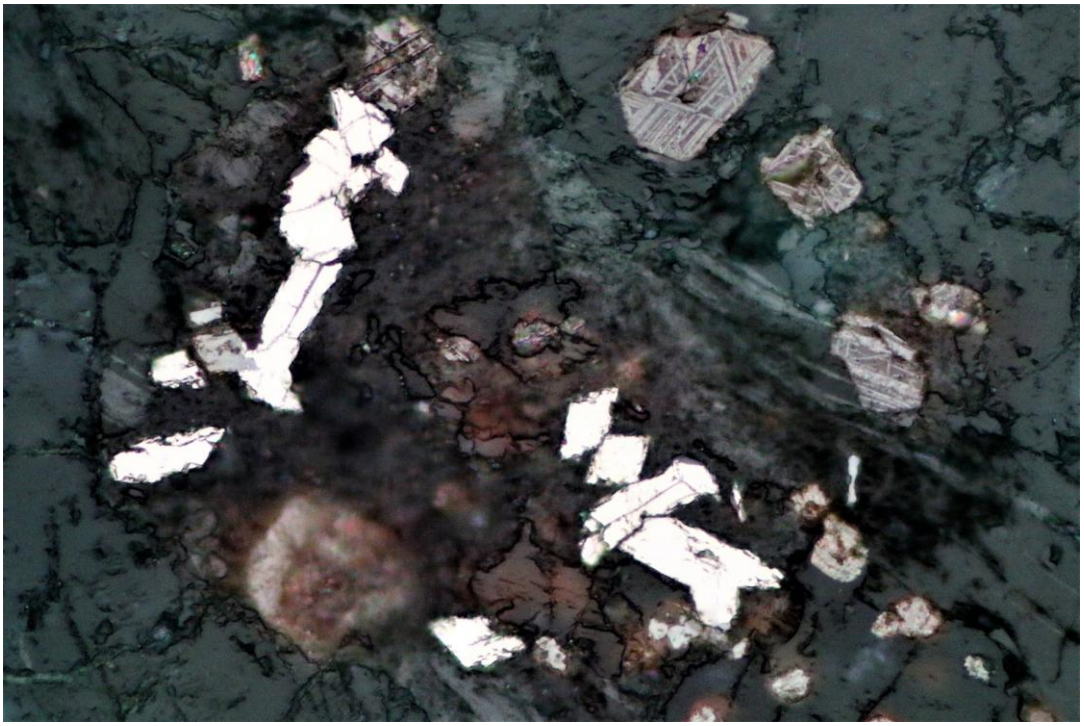

Figure 3. Single and twinned euhedral grains and radially grown crystal aggregates of ferroselite (bright cream) grown inside a host rock fragment (cf. Figure 1). Next to them (upper right) are titanomagnetite pseudomorphs (cf. Figure 2b). Polished section, plane polarized reflected light digital image, width 200 μm.

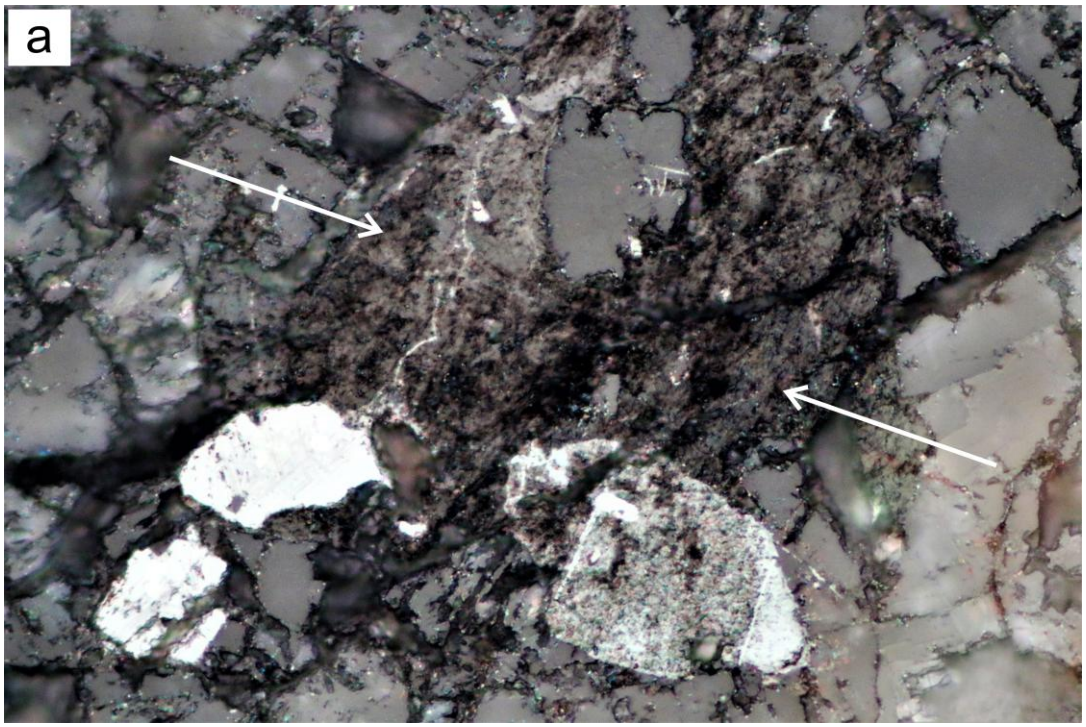

Figure 4. *Cont*.

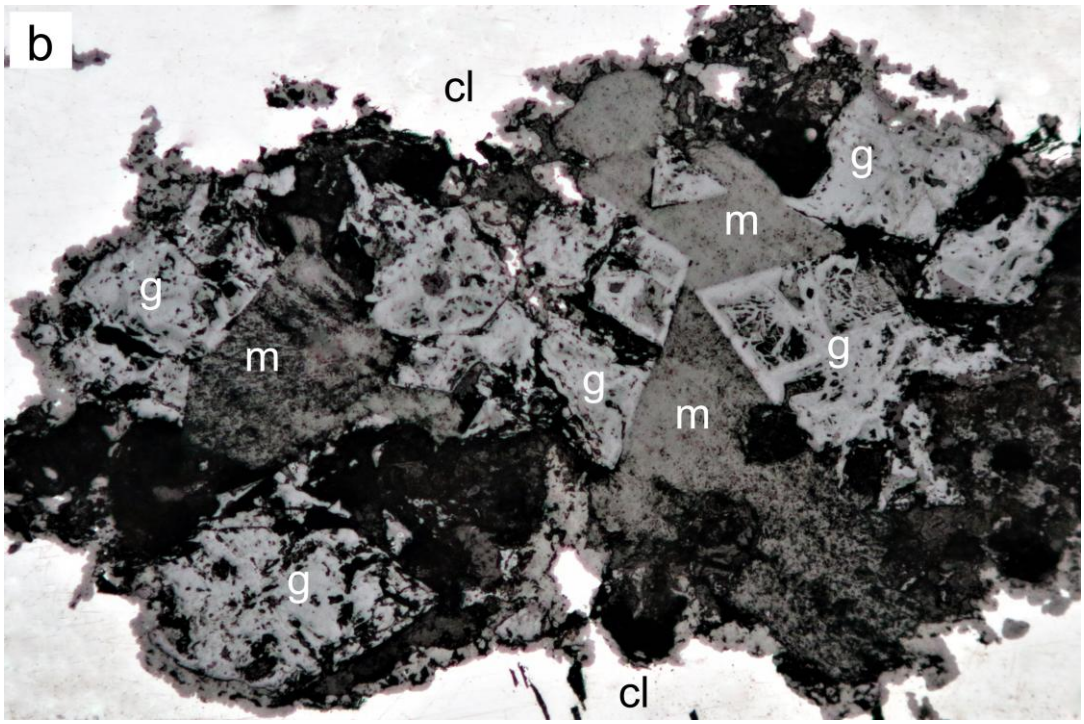

Figure 4. (**a**) Irregular dark-brown patches of bitumen (see white arrows) as fracture fillings cementing the host-rock fragments from the vein wall inwards (cf. Figure 5d). The bright grains are pseudomorphs of TiO_2 after titanomagnetite. Polished section, plane polarized reflected light digital image, width 200 µm; (**b**) Goethite (g) pseudomorph after ankerite (?) cemented by acicular malachite (m) embedded in clausthalite (cl, white). Polished section, reflected light image, width 1 mm, plane polarized light.

3.2. The Cacheuta Vein-Type Se Mineralization

3.2.1. Mineralogy and Structural Features

The selenium mineralization represents a strongly foliated, ductile-deformed, partially brecciated and cavernous fault filling that cuts the trachytic host rock. The main selenide minerals present in variable amounts are clausthalite, klockmannite, eucairite, eskebornite and naumannite, forming a banded or isoclinally folded tectonic mélange (Figures 1 and 5a–d). Grain size ranges between 0.001 and 0.01 mm; grains that survived ductile deformation rarely approach 1 mm in diameter. Our investigation of the 1 to 2-cm-thick selenium veinlets reveals four types of selenide assemblages with regard to the modal abundance of the main selenides (Table 1, Types 1–4), in addition to a Type 5 calculated from published data [1,2]. Vein types 1–4 are shown in Figure 5a–d.

Table 1. Estimated modal percentages of selenides in the five types of Se veinlets.

Mineral	Type 1	Type 2	Type 3	Type 4	Type 5
Eucairite	70	30	<1	<1	7
Clausthalite	5	40	75	50	25
Klockmannite	20	15	5	45	25
Naumannite	4	13	2	<1	<1
Umangite	<1	<1	<1	<1	40
Eskebornite	1	2	15	2	2
Tyrrellite	<1	<1	2	<1	<1
Krut'aite	<1	<1	1	2	1
Trogtalite	<1	<1	<1	<1	<1
Petříčekite	<1	<1	<1	<1	?

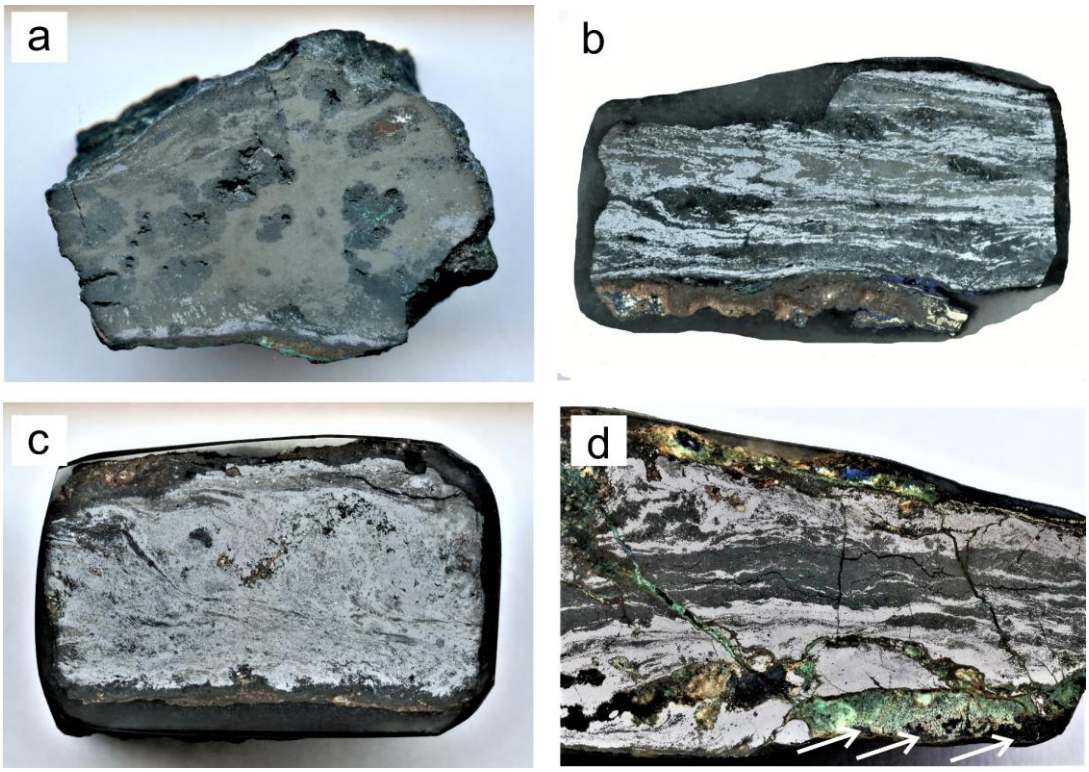

Figure 5. (**a**) Dispersed-light dark field image of Se-veinlet Type-1 (1.7-cm-thick, 2.3-cm-wide, surface rolling grinded, with 1200 mesh SiC abrasive) with eucairite (olive brown) as the main selenide interspersed with irregularly shaped pores inside patchy aggregates of naumannite and klockmannite (dark grey). Clausthalite (light grey) occurs prevalently in thin layers at the vein wall. Notably, the ductile deformation with lineation of the selenides is limited to the vein selvage; (**b**) Dispersed light dark field image of Se-veinlet Type-2 (1-cm-thick, 2.1-cm-wide, embedded in resin, surface rolling grinded, with 1200 mesh SiC abrasive) with eucairite (olive brown) showing a strongly foliated and folded mélange of naumannite and klockmannite (dark grey), clausthalite (light grey) and eucairite (olive brown). The vein selvage contains remnants of chalcopyrite (bright yellow) and as alteration products goethite (dark brown) and malachite (green); (**c**) Dispersed-light dark field image of Se-veinlet Type-3 (1.5-cm-thick, 2.5-cm-wide, embedded in resin, surface rolling grinded, with 1200 mesh SiC abrasive) with a strongly foliated and folded mélange of eskebornite (light brown), klockmannite (dark grey), clausthalite (light grey), and naumannite. The vein selvage contains goethite as the main alteration product (brown). Also shown are partly rotated spotty aggregates of trachytic host-rock fragments; (**d**) Dispersed-light dark field image of Se-veinlet Type-4 (detail from Figure 1, 2.2-cm-thick, 4-cm-wide, embedded in resin, surface rolling grinded, with 1200 mesh SiC abrasive) with layers and lenses of klockmannite (dark grey) and clausthalite (light grey) showing a strongly foliated and folded mélange. Vein selvage, host-rock fragments, and diagonal fractures are stained by goethite (dark brown), azurite and chalcomenite (blue), and malachite (green). Bitumen rarely occurs as irregularly distributed cement impregnating host-rock fragments from the vein wall inwards (see white arrows).

The mineralization consists of strongly foliated, lineated selenide assemblages that precipitated in discrete ductile shear zones. The selenides show evidence of dominant ductile flow and strain accumulation that is higher than that of the adjacent trachytic host rock (Figures 1 and 5a–d). Feldspar grains and larger host rock fragments inside the Se veins have generally survived ductile deformation, in contrast to the selenides. Carbonate minerals (calcite and dolomite), which constitute the gangue in many selenide deposits, were not observed in any of our samples. However, a carbonate gangue may have initially been deposited in the Cacheuta Se veins as implied from a single fragment of

a pseudomorph of goethite after dolomite (?), ankerite (?), or siderite (?), embedded in a matrix of clausthalite (white) and malachite (grey) (Figure 4b).

The complete list of minerals identified during this study is provided in Figure 6. From the species previously reported in Cacheuta, both achavalite and berzelianite were not detected, corroborating the observations of modern studies of this occurrence [1]. As inferred from this list, Cacheuta hosts several undiscovered, extremely rare, or even new species among the alteration mineral assemblage (highlighted by question marks), which deserve special attention in future studies. The small grain size of these species, together with an intimate intergrowth with neighboring minerals, precluded their collection of XRD-structural data (see below Section 3.2.2).

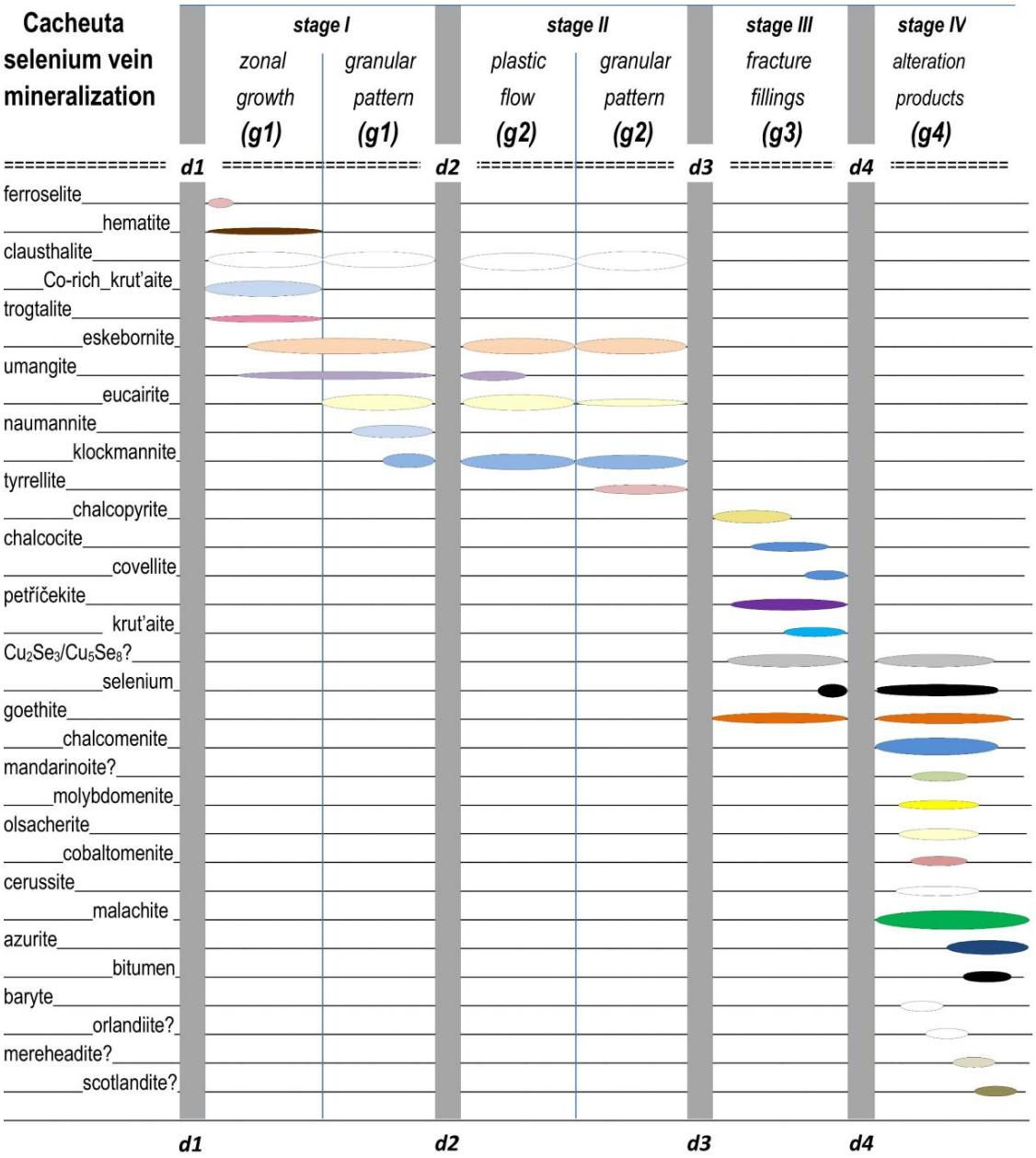

Figure 6. Paragenetic sequence and crystallization/deformation diagram for the Sierra de Cacheuta selenium mineralization.

The formation of the Cacheuta Se occurrence involved grain-size reduction of the coarser-grained precursor selenides. The shapes and arrangements of isoclinal folds reflect the sense of shear. Rarely,

small crystal pockets of very early formed selenides in host rock fractures remained unaffected from the subsequent ductile deformation.

Post-selenide cataclasis cut randomly through all the previous mineralization and deformation structures and opened spaces between the selenium vein and the trachytic host that were partly or completely filled with copper sulfides. All of the selenium veinlets experienced strong overprinting, with goethite, malachite, azurite, chalcomenite, and molybdomenite as the most common alteration minerals.

3.2.2. Micro-Structural Features

Figure 6 provides a summary of microtextural evidence for the relationship between selenide growth and the sequence of deformation, precipitation, and alteration.

Three stages of selenide precipitation (stage (**I**), stage (**II**), and stage (**III**)) and one stage of alteration (stage (**IV**)), triggered by three brittle deformational events (deformation (*d*1), deformation (*d*3), and deformation (*d*4)) and one major ductile deformational event (deformation (*d*2)), could be distinguished and are described hereafter according to its inferred age sequence (Figure 6):

- Deformation (*d*1): First vein opening and brecciation of the trachytic host rock.

  Stage (**I**) corresponds to the zonal and granular growth generation (g1) cementing host rock fragments.
- Deformation (*d*2): Compression and subsequent shearing of stage (**I**) selenides causing foliation and isoclinal folding.

  Stage (**II**) corresponds to the crystal-plastic flow, rotation, dissolution, replacement, and/or recrystallization of stage (**I**) selenides.
- Deformation (*d*3): Second vein opening, fragmentation of stage (**I**) and (**II**) selenides

  Stage (**III**) corresponds to the growth generation (g3) of Cu–Fe sulfides and the formation of major shrinking cracks in selected selenides.
- Deformation (*d*4): Fourth vein opening, fragmentation of stage (**I**)–(**III**) aggregates.

  Stage (**IV**) corresponds to the intensive alteration of pre-existing selenides and the formation of various alteration minerals, resulting in growth generation (g4), cementing all previous structures.

Brittle deformation (*d*1) caused the opening of the fracture zone and subsequent fluid flow into the open spaces of the trachytic host rock, giving rise to stage (**I**) selenide precipitation. The earliest generation of krut'aite-(g1), trogtalite-(g1), clausthalite-(g1), eskebornite-(g1), umangite-(g1), eucairite-(g1), naumannite-(g1), and klockmannite-(g1) partly cemented and/or corroded the fine-grained feldspar and hematite fragments of the host rock along the grain boundaries (Figure 7). Pseudomorphs after cubic crystal forms (cubes, octahedra, and cuboctahedron) occur prevalently in klockmannite-, eskebornite-, and clausthalite-rich layers and lenses. These forms (ca. 20 vol %) are frequently outlined by isolated relics of krut'aite and trogtalite and newly grown tyrrellite (Figures 8–10). We interpret these structures as the earliest krutaite-(g1) generation (with up to six optically distinguishable zones of max. 20 µm thickness) that was deposited in oscillating alternation with trogtalite-(g1) and crystallized as euhedral to subhedral grains or coatings grown from the vein wall inwards, followed by the other (g1) selenides (Figures 8 and 9). In addition to the observations made during this study, Paar et al. (2016) [1] reported inclusions of umangite with oriented "spindle-shaped? exsolution lamellae" of eucairite and klockmannite, which also formed during stage (**I**) and make up Se vein Type 5 (cf. Table 1).

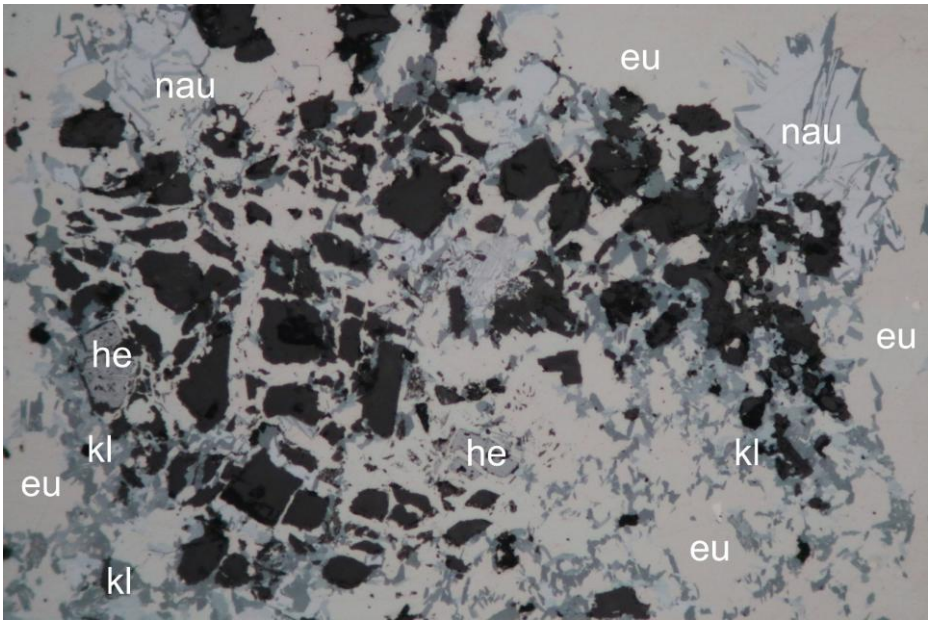

Figure 7. Detail from Se vein Type 1: A granular aggregate of eucairite (eu), klockmannite (kl), and naumannite (nau) is partially replacing a host rock fragment along the grain boundaries of K-feldspar (black) and hematite (he, grey). Reflected light image, 500-µm-wide, plane polarized light.

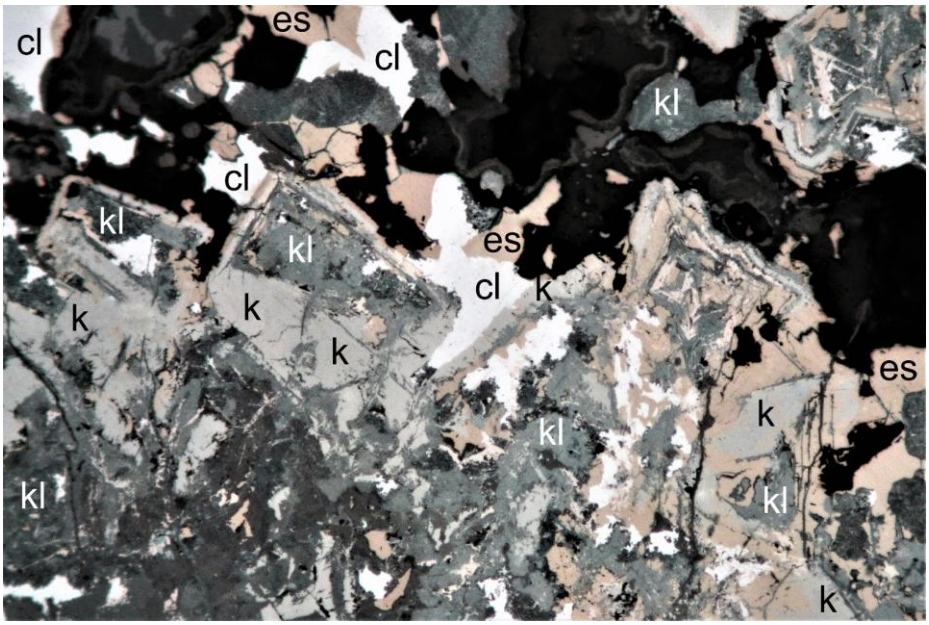

Figure 8. Detail from Se vein Type 3: Few preserved remnants of former subhedral krut'aite-(g1) crystals (k) project into a cavity (black) of the host rock. The originally rectangular shapes of the krut'aite crystals are traced by thin zones of trogtalite-(g1). Patchily distributed replacement and alteration products are klockmannite-(g2) (kl), eskebornite-(g2) (es), and clausthalite-(g2) (cl). Reflected light image, 500-µm-wide, plane polarized light.

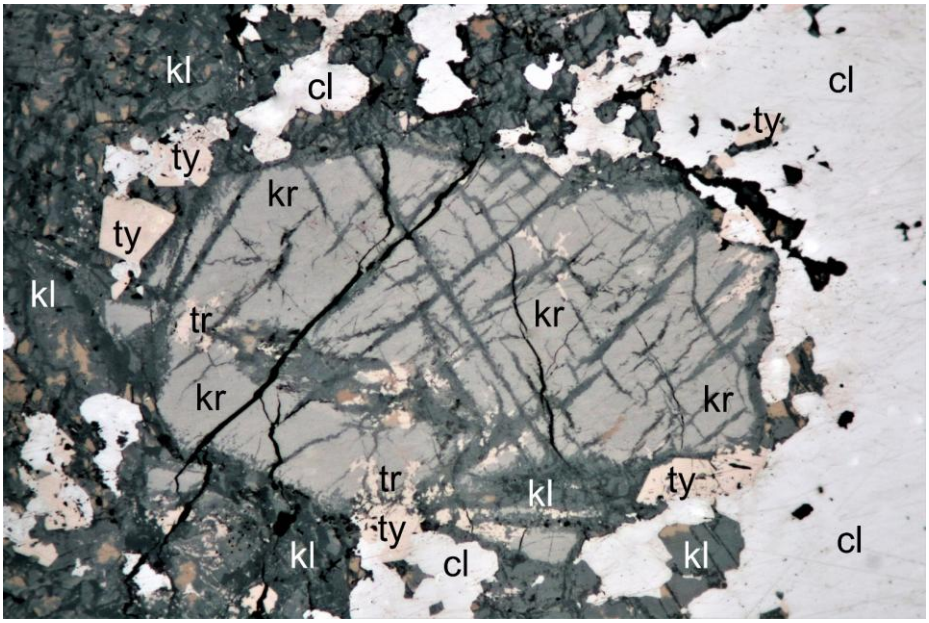

Figure 9. Detail from Se vein Type 3: Replacement relics of krut'aite-(g1) (kr). The original rectangular shapes of the krut'aite crystals are outlined by patchily distributed trogtalite-(g1) (tr) and tyrrellite (g2) (ty). Other replacement and alteration products are klockmannite-(g2) (kl), eskebornite-(g2) (brown spots) and clausthalite-(g2) (cl). Reflected light image, 500-µm-wide, plane polarized light.

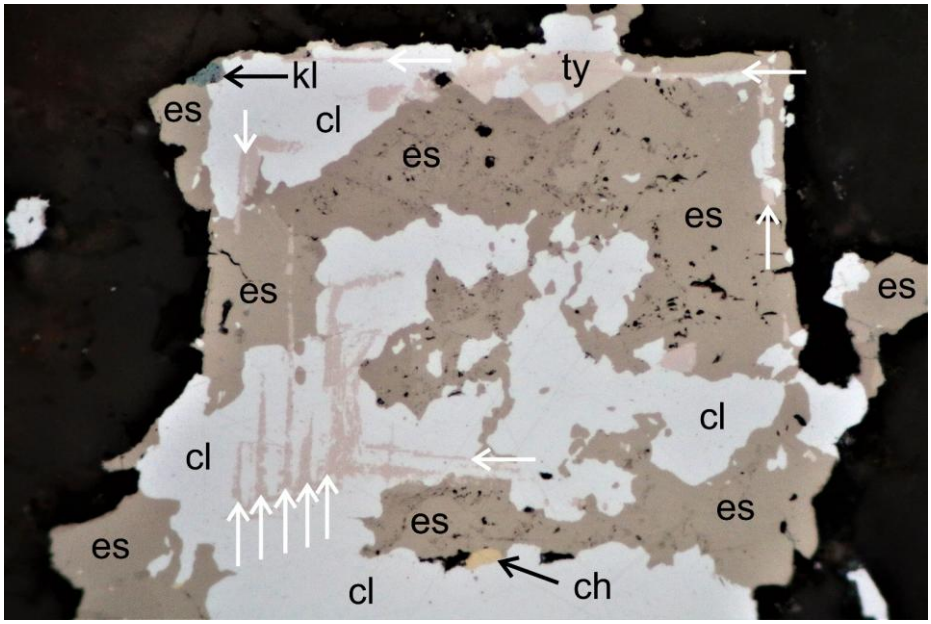

Figure 10. Detail from Se-vein Type-3: Originally cubically shaped and oscillatory grown krut'aite-(g1) crystal traced by thin zones of trogtalite-(g1) (see white arrows). Other replacement and alteration products are klockmannite-(g2) (kl), eskebornite-(g2) (es), clausthalite-(g2) (cl), and chalcopyrite-(g3) (ch). Reflected light image, 200-µm-wide, plane polarized light.

Subsequent compressional stress and shearing (*d*2) caused a strong local ductile deformation, giving rise to foliation, isoclinal folding, and boudinage of the selenides. Formerly brecciated and cemented mineral aggregates were partitioned and rotated. Plastic flow of the grains initiated stage (**II**) selenide overprint involving dissolution, replacement, and/or recrystallization reactions. Rich eucairite

mineralization of Se vein Type 1 generally suffered flattening of granularly textured eucairite (eu), showing a network of extensional fractures outlined by klockmannite (kl), which partially replaced the eucairite along the grain boundaries (Figure 11). Subsequent compression also caused multiple kinkbands in the klockmannite, which were later altered by recrystallization.

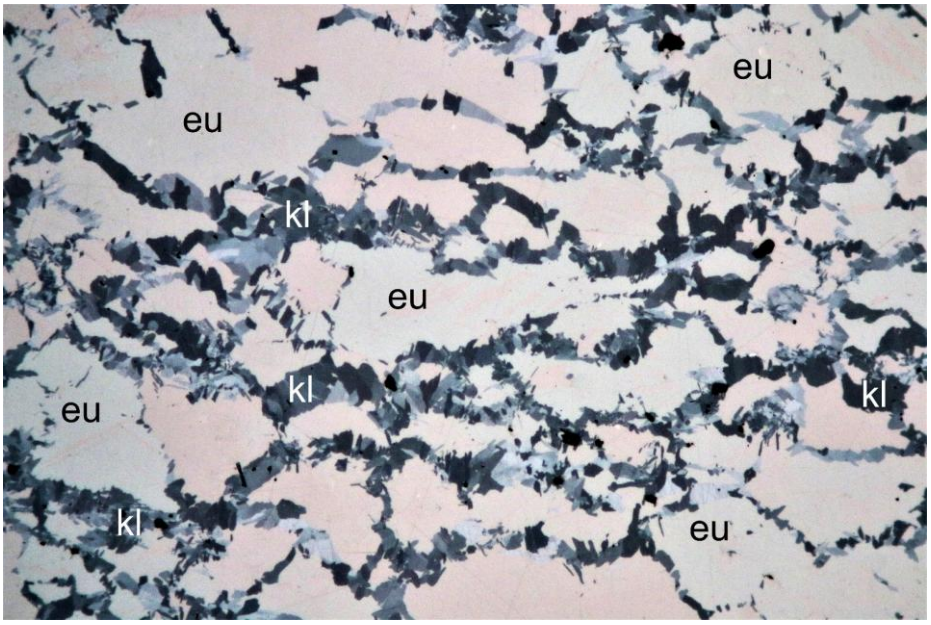

Figure 11. Detail from Se vein Type-1: Flattening of granularly textured eucairite (eu) showing a network of extensional fractures outlined by klockmannite (kl). Subsequent compression created multiple kinkbands in the klockmannite, which were later modified by recrystallization. Reflected light image, 500-µm-wide, plane polarized light.

A syn-tectonic phase was followed by a post-tectonic phase associated with widespread alteration of the earlier mineralization and subsequent growth of post-tectonic mineral aggregates. Fine-grained polygonal aggregates of clausthalite-(g2), eskebornite-(g2), umangite-(g2), eucairite-(g2), naumannite-(g2), and klockmannite-(g2) precipitated. In contrast to previous reports [1,2], the samples studied in this paper contain only tiny, armored relics of umangite-(g1) in hematite-(g1). Due to the intensive ductile overprint, most of the umangite-(g1) became unstable and was replaced by klockmannite-(g2) and clausthalite-(g2).

During stage (**II**), eucairite was replaced by naumannite, klockmannite, and/or clausthalite. Trogtalite was replaced by tyrrellite, eskebornite, clausthalite, and/or klockmannite. Umangite was replaced by hematite, klockmannite, and/or tyrrellite. Eskebornite was replaced by klockmannite, clausthalite, and/or tyrrellite. Notably, large portions of umangite and klockmannite often showed finely branched shrinkage cracks, giving strong evidence that these selenides suffered significant loss of volume [1].

Brittle deformation (*d*3) generated multiple micro-fractures and micro-brecciation preferentially parallel to the selvages and perpendicular to the Se vein (Figure 12). Subsequently, Cu–Fe–S-rich fluids infiltrated the Cacheuta fault system, giving rise to another event of widespread alteration of the earlier mineralization. Late-stage (**III**) sulfides comprising chalcopyrite-(g3), chalcocite-(g3), and covellite-(g3) postdate the (g1)–(g2) selenides. Chalcopyrite, mostly as thin colloform coatings of "blister copper", symmetrically covered and cemented the micro-fractures (Figure 12).

At the end of stage (**III**), the existing shrinkage cracks, micro-fractures, interstices, and porous selenide aggregates were successively invaded by strongly oxidizing fluids, which also attacked the newly precipitated sulfide cement to form goethite-(g4). Pre-existing clausthalite that crystallized at

the margins and outside the complex selenide structure was easily accessible for these fluids, which triggered its partial or complete replacement by a complicated mixture of extremely rare, fine-grained selenides-(g3) including klockmannite-(g3), petříčekite-(g3), krut'aite-(g3), native selenium-(g3) [7] (Figure 13), and two new phases (Figures 14 and 16).

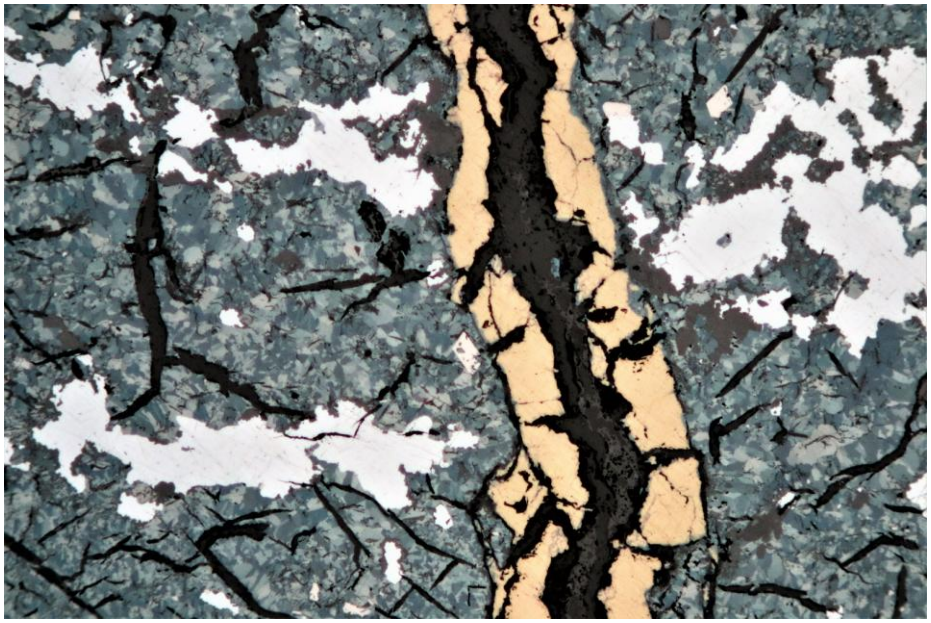

Figure 12. Brittle deformation (*d*3) caused detachment and fragmentation of fine-grained klockmannite (blue-grey) and clausthalite (bright) perpendicular to the vein selvage and flattening of the selenides. Notably, large portions of klockmannite show finely branched shrinkage cracks (black), providing evidence for significant loss of volume. Reflected light image, 1-mm-wide, plane polarized light.

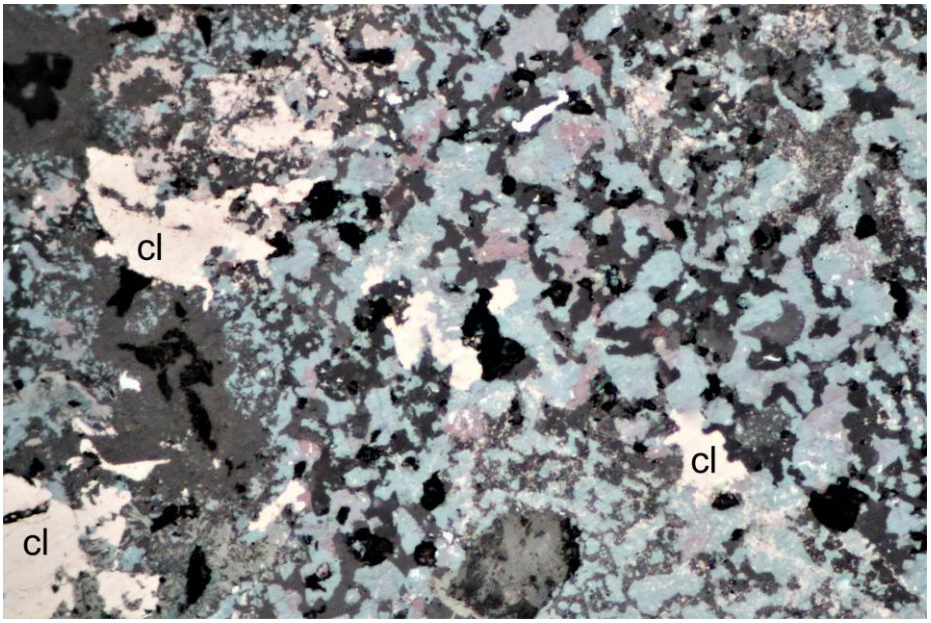

Figure 13. Clausthalite (cl) partly replaced by end-member krut'aite (blue), end-member petříčekite (blue-violet), molybdomenite (dark grey), and native selenium (light grey), forming a myrmecitic texture [7]. Reflected light image, 500-μm-wide, plane polarized light.

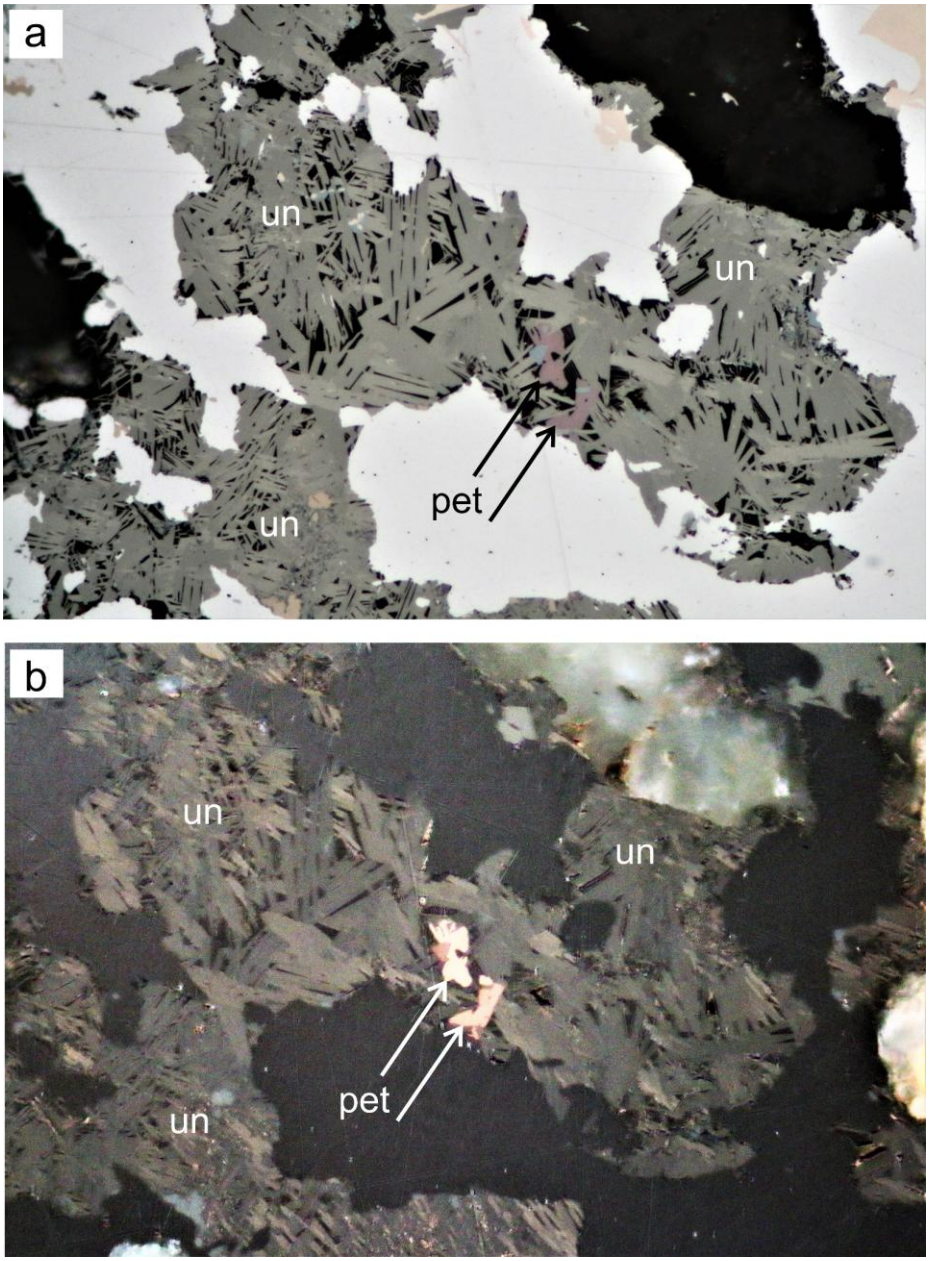

Figure 14. Reflected light images (each 200-μm-wide) of the unnamed Cu selenide (white mineral = clausthalite). (**a**) Plane polarized light; (**b**) crossed polarizers; un = unnamed Cu selenide, pet = end-member petříčekite. For further explanations see text.

One of those new species is a Cu selenide forming an angular network-like intersertal texture of lath-shaped thin plates with solitary inclusions of end-member krut'aite and end-member petříčekite replacing clausthalite, naumannite and eskebornite. Optical properties are shown in Figure 14. In plane-polarized incident light, the mineral is greenish-grey in color, slightly bireflectant and weakly pleochroic from greenish-grey to light grey, showing no internal reflections. Under crossed polarizers, the mineral is weakly anisotropic, with light-brown to dark-grey rotation tints. The selenide always contains several weight percentages of Ag and Pb, which are negatively correlated. In the case that it represents a discrete phase and not a nano-scale mixture of two or more phases, its ideal formula may be either Cu_2Se_3 or Cu_5Se_8.

Moderate post-selenide and post-sulfide cataclasis (*d*4) cut through all existing mineralization and deformation structures and opened space between the selenium vein sections and the trachytic host rock. Stage-(**IV**) of ongoing alteration in the oxidation zone gave rise to a plethora of secondary minerals of growth generation (g4): chalcomenite, molybdomenite (Figure 15), olsacherite, cobaltomenite, cerussite, malachite, native selenium, barite, and several incompletely characterized phases.

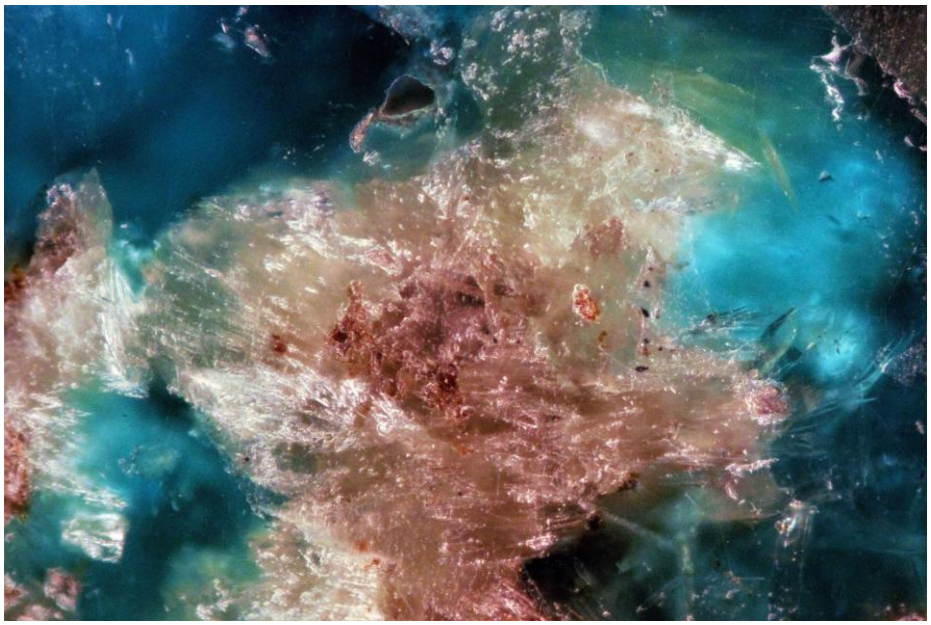

Figure 15. Detail from Se vein Type-4. Dispersed-light dark field image of an acicular aggregate of molybdomenite (colorless transparent) showing internal reflections, partly stained by inclusions of goethite (red-brown,) and surrounded by chalkomenite (blue). Cacheuta is the type locality of chalcomenite and molybdomenite. Width 500 μm.

One of the phases yet unknown from Cacheuta is a Cu–Fe selenite, representing an alteration product of eskebornite (Figure 16). These grains are characterized by strongly varying Cu/Fe ratios, from Cu > Fe to Cu = Fe to Cu < Fe. Possibly, these alteration products represent chalcomenite and ***mandarinoite***, $Fe^{3+}{}_2(SeO_3)_3 \cdot 6H_2O$ [14,15]. Optical properties are shown in Figure 16. In plane-polarized incident light, the mineral is medium to dark grey. The decomposition of the eskebornite grains increasingly developed from bottom to top and showed the state of transformation along the strong cleavage of eskebornite parallel (0001). The direction of the cleavage indicates the spatial position of the individual eskebornite grains. The close subparallel intergrowth of the eskebornite relics and alteration products prevents a more detailed description of their optical properties.

Three other not clearly identifiable species, which are commonly associated with cerussite, constitute different alteration products of clausthalite and attest to the late-stage interaction of the selenides with C–S–Cl–B-bearing fluids. One of those phases mainly consists of Pb, Cl, and Se, together with O and eventually H, and may represent ***orlandiite***, $Pb_3(SeO_3)(Cl,OH)_4 \cdot H_2O$ [16]. In addition to these components, but devoid of Se, the second phase contains B and, if not constituting a new phase, may identify as ***mereheadite***, $Pb_{47}O_{24}(OH)_{13}Cl_{25}(BO_3)_2(CO_3)$ [17]. The third phase is a sulfite and probably resembles ***scotlandite***, $PbSO_3$ [18], the S-analogue of molybdomenite.

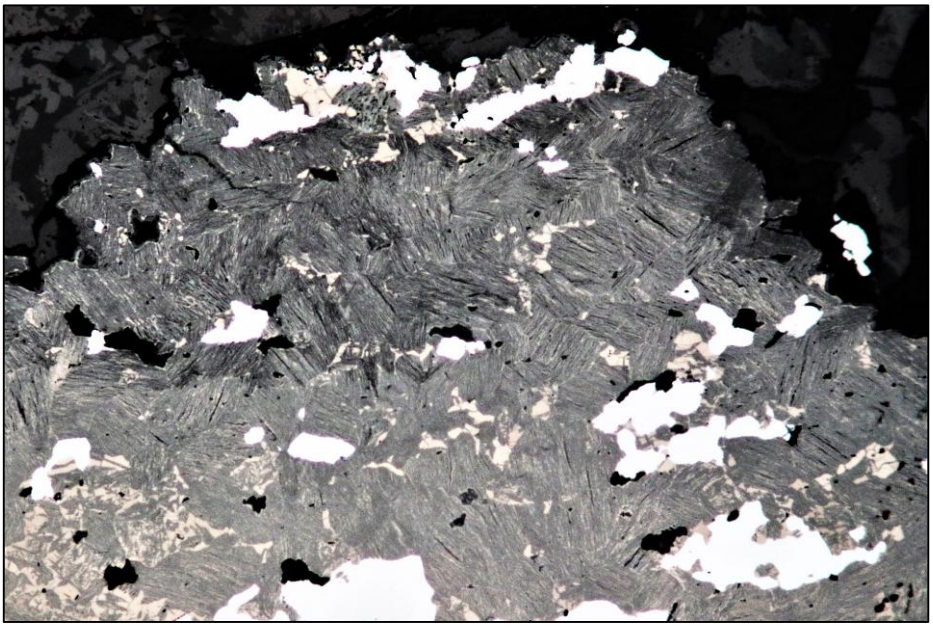

Figure 16. Eskebornite (light-brown) and clausthalite (bright) largely replaced by unknown Cu–Fe selenites (light-grey to dark-grey) of strongly varying Cu/Fe ratios, from Cu > Fe to Cu = Fe to Cu < Fe, possibly representing chalcomenite and mandarinoite. The darker the domains are, the more Fe-rich is the alteration mineral. Reflected light image, 500-µm-wide, plane polarized light.

3.2.3. Mineral Chemistry

Representative results of the electron-microprobe analyses of the selected selenides and sulfides are listed in Tables 2 and 3. Formula proportions reported in the text refer to the main formulas.

Krut'aite-(g1) (cf. Figures 8 and 9) is moderately rich in Co (4.9–6.7 wt %) and contains minor concentrations (in wt %) of Ag (0.5–3.8), Ni (0.4–1.2), and Fe (0.5–1.2) (Table 2, ana# 1–3). The concentrations of the other elements sought are below 0.1 wt %. Its mean formula is $(Cu_{0.71}Co_{0.22}Ag_{0.04}Ni_{0.03}Fe_{0.03})_{\Sigma 1.03}Se_{1.98}$ (n = 6). In the course of later replacement, cobalt, copper and nickel liberated during dissolution of krut'aite-(g1) were concentrated in tyrrellite. The low Ni content was insufficient to crystallize independent nickel selenides as, for example, in El Dragón, Bolivia [19]. Late-formed krut'aite-(g3) (Table 2, ana# 4) has almost end-member composition ($Cu_{0.99}Se_{2.00}$) (n = 3). The only non-ideal cation measured in klockmannite [$(Cu_{0.98}Ag_{0.02})_{\Sigma 1.00}Se_{1.00}$; n = 4] is Ag (0.7–2.2 wt %) (Table 2, ana# 5–6). Near-ideal eskebornite has the mean formula $Cu_{0.99}Fe_{1.01}Se_{1.99}$ (n = 4), with only Ag being detectable as non-stochiometric element (Table 2, ana# 7–8). Late-stage petříčekite has also near-end-member composition, possessing the mean formula $(Cu_{0.98}Fe_{0.01})_{\Sigma 0.99}Se_{2.00}$ (n = 7). It occasionally hosts minor concentrations (in wt %) of Ag (0–0.5), Pb (0–0.4), and Fe (0–0.5).

Eucairite, $Cu_{1.00}Ag_{1.00}Se_{0.99}$ (n = 4), is also very poor in non-ideal elements (Table 3, ana# 1–2). Naumannite has the average formula $(Ag_{0.98}Cu_{0.02})_{\Sigma 1.00}Se_{1.00}$ (n = 7), with some Cu (0.1–1.4 wt %) possibly substituting for Ag (Table 3, ana# 3–4). Clausthalite, $(Pb_{0.97}Cu_{0.04})_{\Sigma 1.01}Se_{0.99}$ (n = 8), may as well have incorporated minor Cu (0.1–1.7 wt %) (Table 3, ana# 5).

Table 2. Representative results of the electron-microprobe analyses of krut'aite, klockmannite, eskebornite, and petříčekite.

Element/#	1	2	3	4	5	6	7	8	9	10	11
Cu (wt %)	18.37	20.19	20.78	28.48	42.87	44.09	22.66	22.67	28.32	27.78	28.11
Ag	3.80	1.50	0.89	b.d	2.24	0.73	0.19	0.16	b.d	b.d	0.53
Pb	0.06	0.06	0.09	b.d	b.d	b.d	b.d	b.d	0.11	0.40	0.20
Fe	0.64	0.50	1.15	0.05	b.d	b.d	20.33	20.45	b.d	0.21	0.48
Co	5.99	6.69	6.11	0.11	b.d	b.d	b.d	b.d	b.d	b.d	b.d
Ni	1.22	0.45	0.47	b.d	b.d	b.d	b.d	b.d	b.d	b.d	b.d
S	0.04	0.04	0.05	0.03	b.d	b.d	b.d	b.d	b.d	0.06	0.06
Se	70.73	70.78	70.97	71.17	55.59	55.67	56.40	56.67	71.33	71.61	70.99
Total	100.85	100.21	100.51	99.84	100.70	100.50	99.58	99.92	99.76	100.06	100.34

Notes: b.d. = below detection limit; 1–4 = krut'aite, 5–6 = klockmannite, 7–8 = eskebornite, 9–11 = petříčekite.

Table 3. Representative results of electron-microprobe analyses of eucairite, naumannite, clausthalite, tyrrellite, and trogtalite.

Element/#	1	2	3	4	5	6	7	8	9	10	11
Cu (wt %)	25.44	25.53	0.74	1.36	1.72	12.86	12.90	12.75	4.17	7.48	6.20
Ag	43.59	43.27	72.43	71.74	0.09	b.d	b.d	b.d	0.08	0.95	0.35
Hg	0.14	b.d.	b.d.	0.28	b.d.	b.d.	b.d.	b.d.	b.d.	b.d.	b.d.
Pb	b.d.	0.08	b.d.	b.d.	70.19	b.d.	b.d.	0.08	b.d.	b.d.	b.d.
Fe	b.d.	b.d.	b.d.	b.d.	b.d.	0.09	0.12	0.08	0.38	0.78	0.31
Co	b.d.	b.d.	b.d.	b.d.	0.06	22.38	22.33	20.83	21.80	19.82	21.66
Ni	b.d.	b.d.	b.d.	b.d.	b.d.	0.74	1.19	2.72	1.23	b.d.	b.d.
S	b.d.	b.d.	b.d.	b.d.	b.d.	0.31	0.22	0.09	0.17	0.10	0.09
Se	31.35	31.25	27.02	27.01	28.46	63.19	63.16	63.33	72.01	71.33	71.74
Total	100.52	100.14	100.19	100.39	100.52	99.57	99.92	99.89	99.84	100.46	100.35

Notes: b.d. = below detection limit; 1–2 = eucairite, 3–4 = naumannite, 5 = clausthalite, 6–8 = tyrrellite, 9–11 = trogtalite.

Non-ideal components present in tyrrellite comprise Ni (0.5–2.7 wt %) and S (0.1–0.3 wt %) (Table 3, ana# 6–8). Silver, Hg, Pb, and Fe were occasionally measured at low concentrations. It has the mean formula $Cu_{1.00}(Co_{1.87}Ni_{0.11}Fe_{0.01})_{\Sigma 1.99}(Se_{3.98}S_{0.03})_{\Sigma 4.01}$ (n = 18). The replacement mineral trogtalite, $(Co_{0.79}Cu_{0.19}Fe_{0.02}Ag_{0.01}Ni_{0.01})_{\Sigma 1.02}(Se_{1.97}S_{0.01})_{\Sigma 1.98}$ (n = 9), is moderately rich in Cu (4.1–7.5 wt %) and notoriously contains minor Ag (0.1–1.0 wt %), Fe (0.1–0.9 wt %) and S (0.1–0.2 wt %) (Table 3, ana# 9–11).

A single spot was conducted on a final-stage sulfide (i.e., the chalcopyrite grain included in the krut'aite pseudomorph shown in Figure 10). This grain is rich in Se (16.4 wt %) and exhibits the formula $Cu_{0.99}Fe_{0.99}(S_{1.59}Se_{0.43})_{\Sigma 2.02}$.

Plotting the compositions of trogtalite, krut'aite, and tyrrellite in the Co–Ni–Cu ternary diagrams representing the systems $(Co,Ni,Cu)Se_2$ and $(Co,Ni,Cu)_3Se_4$ reveals chemical signatures that mostly deviate from those reported from other Se occurrences (Figures 17 and 18) and, thus, constitute diagnostic features for this site.

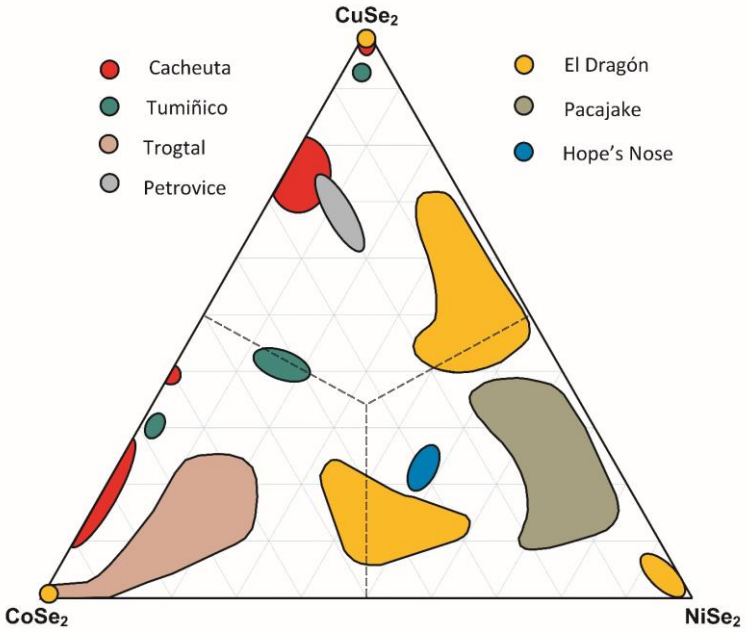

Figure 17. Co–Ni–Cu ternary diagram (mole %) of the system trogtalite–penroseite–krut'aite. Data sources: Cacheuta ([1,2], this paper), Tumiñico [1,2], Trogtal [2,20], Petrovice [21], El Dragón [4,19,22,23], Pacajake [19,22–24], and Hope's Nose [24,25].

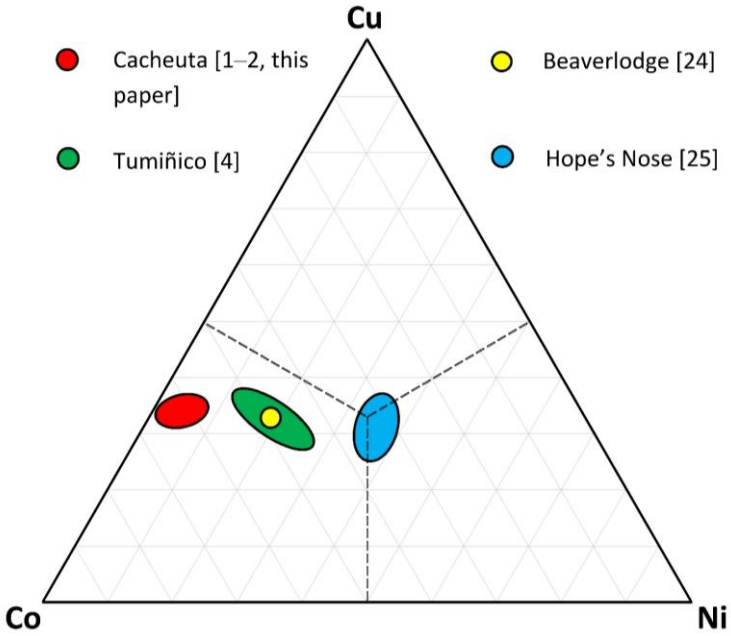

Figure 18. Co–Ni–Cu ternary diagram (mole %) of the system $(Co,Ni,Cu)_3Se_4$.

4. Discussion

4.1. Sources of Elements

Inferences regarding the possible sources of selenium and the accompanying elements could only be made from brief historic descriptions of the local geology and information that is provided by sample materials that unequivocally relate to the Cacheuta mineralization.

Despite these strong limitations in knowledge, the bituminous shales intercalated in various sedimentary rocks in the vicinity of the Se veins recognized by [9] are the prime candidates for the

major source of Se and the accompanying metals. Note that bitumen is also noted as constituent of the Se veins ([11], this paper). Suggesting these shales as elemental source is speculative, because we know practically nothing about their extent, composition, and mineralogy. However, black shales and coals are typically rich in framboidal pyrite and organic matter and are globally known as important carriers of a large suite of metals, including selenium [26–31].

It is our suspicion that black shales in the vicinity of the Se veins likely acted as the major host rock for the elements that are immobilized in the various crystallized selenides at Cacheuta. Processes involving highly oxidized fluids have likely (a) oxidized and dissolved Se-containing sulfide minerals and (b) mobilized absorbed and organic-bound selenium. During interaction with these fluids, reduced selenide (Se^{2-}) became oxidized to selenate (Se^{6+}), capable of migrating and depositing outside of the host. Selenate was again reduced to selenite or even native selenium when the migrating fluids lost their oxidation potential through interaction with reductants, triggering the deposition of the primary Se species at this site.

4.2. Origin of Se Mineralization

Considering the thermodynamic properties of binary selenides at T = 100 °C and elevated oxygen fugacities [32], the absolute and relative oxygen, selenium, and sulfur fugacities of the fluids during the different stages of formation of the Cacheuta mineralization could have been constrained. The presence of hematite in the earliest stage (**I**) implies that the f_{O2} was above the hematite–magnetite buffer. Moreover, formation of ferroselite suggests that the oxygen fugacity was still considerably higher at the onset of Se mineral precipitation, at least about 5.8 log units above the hematite–magnetite buffer [32]. At such strongly elevated oxygen fugacity, the absence of berzelianite indicates that the $\log f_{Se2}$ was above that defined by the berzelianite–umangite univariant reaction, (i.e., exceeded −14.5) which also permitted the crystallization of Co-rich krut'aite. The lack of pure krut'aite and the crystallization of klockmannite implies that the Se fugacity in the fluids remained below the klockmannite–krut'aite buffer (i.e., $\log f_{Se2}$ was less than −11.2). This range in Se fugacity prevailed until the end of stage (**II**). Accordingly, the lack of sulfides implies that $\log f_{S2}$ was a maximum of −22 (i.e., the Se/S fugacity was greater than unity throughout both stages). At the beginning of stage (**III**), the short-term precipitation of Se-rich chalcopyrite indicates that the S fugacity in the fluid was a little higher than in the preceding stages, possibly amounting to $\log f_{S2}$ between −22 and −19. As evidenced by the formation of stoichiometric krut'aite and native selenium, the Se fugacity remained high, exceeding the value defined by the krut'aite–native selenium univariant reaction ($\log f_{Se2}$ of −11.2 at T = 100 °C) (i.e., the Se/S fugacity was still greater than unity until the end of the deposition of the fracture-filling selenides at Cacheuta).

4.3. Diagnostic Features of Cacheuta, Mendoza, Compared to the Se Deposits of the Province of La Rioja

As pointed out in the Introduction, there is occasionally confusion about the correct assignment of Se-bearing samples from the Mendoza and La Rioja Provinces in Argentina (Table 4, Figure 19).

Figure 19 highlights the characteristic differences in the vein structure between the Se-mineralization of Sierra de Cacheuta, Mendoza Province, and of the La Millionara Mine, Sierra de Cacho District, which is representative for the Se occurrences of the Province of La Rioja.

Based on historic descriptions, the investigation of historical reference samples, and the most recent review of Argentinian Se deposits [1], we propose the following features as diagnostic for the Cacheuta selenide samples:

(1) Occurrence of trachytic host rock fragments containing ferroselite, bitumen, and TiO_2 pseudomorphs after titanomagnetite.
(2) Several thin zones of trogtalite in Co-rich krut'aite-(g1) (Co < 6.7 wt %) pseudomorphs, representing several stages of selenide deposition.

(3) The selenides show striking evidence of dominant ductile flow, recrystallization, and strain accumulation exceeding that in the adjacent trachytic host rock that only suffered brittle deformation.
(4) Early, Co-rich krut'aite (originally comprising up to 20 vol % of the selenides) is largely replaced by clausthalite, umangite, klockmannite, eskebornite, Ni-poor tyrrellite (Ni < 2.7 wt %) and trogtalite (Ni < 1.2 wt %), as well as krut'aite and petříčekite of end-member composition.
(5) Calcite gangue, Hg–selenides (tiemannite), berzelianite, and native gold are lacking.
(6) Formation of numerous Se-bearing alteration minerals, possibly including mandarinoite, mereheadite, orlandiite, and scotlandite.
(7) Presence of an unnamed Cu selenide (ideal formula either Cu_2Se_3 or Cu_5Se_8).

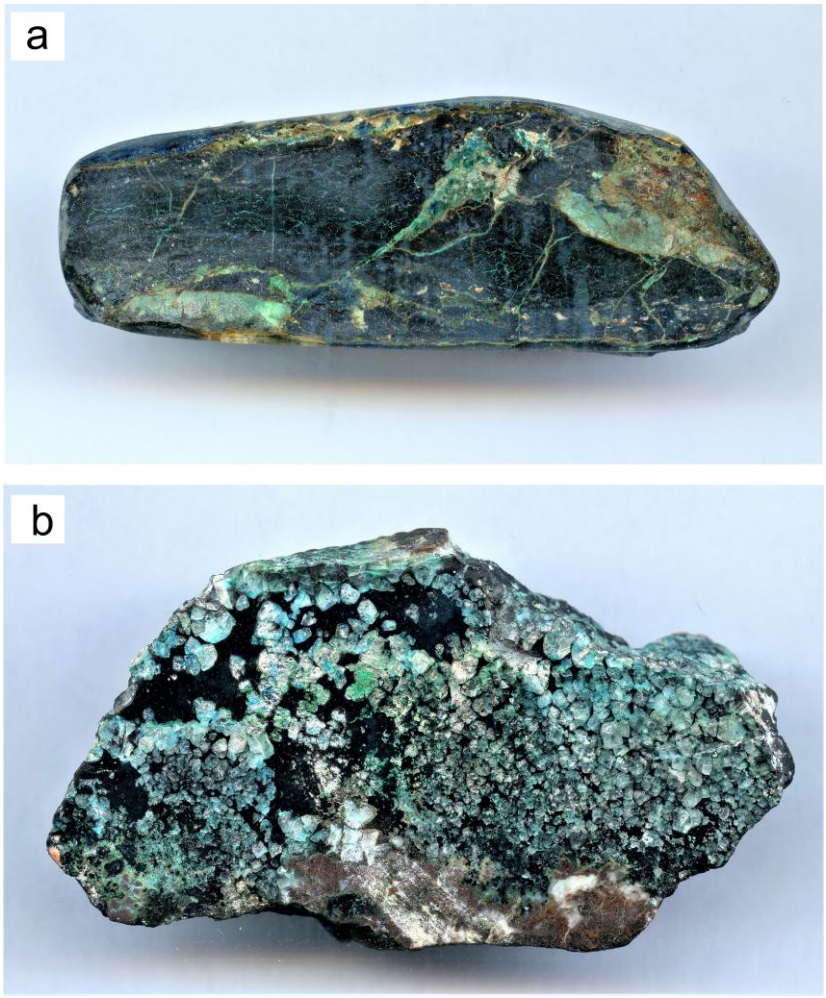

Figure 19. (**a**) Dispersed-light dark field image of Se-veinlet Type-4 from Sierra de Cacheuta (2.2-cm-thick, 6.6-cm-wide, embedded in resin, polished surface). The opaque metallic selenides appear black. Vein selvage, host-rock fragments and diagonal fractures are stained by various alteration products like goethite (dark brown), azurite and chalcomenite (blue), and malachite (green). (**b**) Dispersed-light dark field image of a representative Se-veinlet sample from the La Millionara Mine, Sierra de Cacho District, Province of La Rioja (3.8-cm-thick, 7.1-cm-wide, polished surface). The undeformed Se mineralization (black) consists of umangite, berzelianite and klockmannite. The selenides cement the euhedral crystals (average grain size 2 mm) and crystal aggregates of calcite (white), which are intensively stained by chalcomenite (blue) and malachite (green). Collection F.N. Keutsch, Harvard University, Cambridge, MA, USA.

Table 4. Compilation of the most important Se occurrences of the provinces of La Rioja and Mendoza, Argentina [1]. Mineral species documented in color images by [1] are given in italics.

(1)	**La Rioja Province**
(a)	Los Llantenes district—most important mines: El Chire (*naumannite*, *tiemannite*, *native gold*, *chrisstanleyite*, *jagüétite*, *calcite*); San Pedro (*naumannite*, *eucairite*, *tiemannite, calcite*, *clausthalite*, *hematite*); El Portezuelo; Luis; La Ramada
(b)	Sierra de Cacho district (former, "Sierra de Umango")—most important mines: El Quemado (*umangite*, *ferroselite*, *hematite*); Las Asperezas (*native selenium*, *eucairite*, *naumannite*, *fischesserite*, *native gold*); El Tolar; El Hoyo; La Millionara (*berzelianite*, *klockmannite*, *hematite*, *calcite*)
(c)	Cerro Cacho (northern part of the Sierra de Cacho district)—most important mines: Tumiñico (*native selenium*, *native gold*, *tiemannite*, *umangite*, *klockmannite*, *clausthalite*, *eskebornite*, *brodtkorbite*, *crookesite*, *hakite*, *bucovite*, *chaménaite*, *cadmoselite*, *ferroselite*, *graphite*, *chalcomenite*, *tyrrellite*, *calcite*, *hematite*, *malachite*); *Pichanas* (*umangite*, *klockmannite*)
(d)	Sañiogosta district—most important mines: Santa Brigida (*stilleite, umangite*); La Piedra Pintada
(e)	Sierra de Famatina—most important mine [1]: San Francisco (*umangite, eldragónite, calcite*)
(2)	**Mendoza Province**
(a)	Sierra de Cacheuta (*clausthalite, eucairite, umangite, tyrrellite–bornhardtite, eskebornite, klockmannite, trogtalite, krut'aite*)

Acknowledgments: We are indebted to Frank N. Keutsch for loaning the specimens from Cacheuta and sharing his scientific expertise on this occurrence. Two anonymous reviewers provided valuable suggestions.

Author Contributions: Günter Grundmann manufactured the polished sections, performed the microstructural analysis, and determined the genetic sequence of the mineral deposition and alteration. Hans-Jürgen Förster conducted the electron-microprobe analyses. Hans-Jürgen Förster and Günter Grundmann wrote the paper.

Conflicts of Interest: The authors declare no conflict of interest.

References

1. Paar, W.H.; de Brodtkorb, M.K.; Putz, H.; Martin, R.F. *Atlas of Ore Minerals: Focus on Epithermal Deposits of Argentina*; Mineralogical Association of Canada: Québec, QC, Canada, 2016; Volume 11, p. 408.
2. Paar, W.H.; Sureda, R.J.; de Brodtkorb, M.K. Mineralogía de los yaciminientos de selenio en La Rioja, Argentina. Krutaita, tyrrellita y trogtalita de Los Llantenes. *Rev. Assoc. Geol. Argent.* **1996**, *51*, 304–312.
3. Paar, W.H.; Amann, G.; Topa, D.; Sureda, R.J. Gold and palladium in the Sierra de Umango and Los Llantenes selenide districts, La Rioja, Argentina. In Proceedings of the Memoria del XIV Congreso Geologico Boliviano, La Paz, Bolivia, 14–18 November 2000; pp. 465–469.
4. Paar, W.H.; Topa, D.; Roberts, A.C.; Criddle, A.J.; Amann, G.; Sureda, R.J. The new mineral species brodtkorbite, Cu_2HgSe_2, and the associated selenide assemblage from Tuminico, Sierra de Cacho, La Rioja, Argentina. *Can. Mineral.* **2002**, *40*, 225–237. [CrossRef]
5. Paar, W.H.; Topa, D.; Makovicky, E.; Sureda, R.J.; de Brodtkorb, M.H.; Nickel, E.H.; Putz, H. Jagüeite, $Cu_2Pd_3Se_4$, a new mineral species from El Chire, La Rioja, Argentina. *Can. Mineral.* **2004**, *42*, 1745–1755. [CrossRef]
6. De Brodtkorb, M.K.; Crosta, S. Sobre los yaciemientos de Se de la "Sierra de Umango", provincia de la Rioja. *Rev. Assoc. Geol. Argent.* **2010**, *67*, 272–277.
7. Bindi, L.; Förster, H.-J.; Grundmann, G.; Keutsch, F.N.; Stanley, C.J. Petříčekite, $CuSe_2$, a new member of the marcasite group from the Předbořice deposit, Central Bohemia Region, Czech Republic. *Minerals* **2016**, *6*, 33. [CrossRef]
8. Stelzner, A. *Beiträge zur Geologie und Palaeontologie der argentinischen Republik: Geologischer Teil*; Palaentographica; Suppl. 3; Theodor Fischer: Berlin, Germany, 1885.
9. Stelzner, A. Mineralogische Beobachtungen im Gebiete der argentinischen Republik. *Tschermak's Min. Mitt.* **1873**, 219–254.
10. Domeyko, I. *Excursiones y Trabajos Entre 1840–1873*; Geología San Félix veta Descubridora: Chañarcillo, Chile, 1873.
11. Brackebusch, L. Die Bergwerksverhältnisse der argentinischen Republik. *Zeitschrift Berg- Hütten- und Salinenwesen* **1893**, *41*, 15–47.

12. Ramdohr, P. *Die Erzmineralien und ihre Verwachsungen*; Akademie-Verlag: Berlin, Germany, 1975; p. 904.
13. Armstrong, J.T. CITZAF: A package of correction programs for the quantitative electron microbeam X-ray-analysis of thick polished materials, thin films, and particles. *Microbeam Anal.* **1995**, *4*, 177–200.
14. Dunn, P.J.; Peacor, D.R.; Sturman, B.D. Mandarinoite, a new ferric-iron selenite from Bolivia. *Can. Mineral.* **1978**, *16*, 605–609.
15. Hawthorne, F.C. The crystal structure of mandarinoite, $Fe^{3+}{}_2Se_3O_9{\cdot}6H_2O$. *Can. Mineral.* **1984**, *22*, 475–480.
16. Camprostrini, I.; Gramaccioli, C.M.; Demartin, F. Orlandiite, $Pb_3(SeO_3)(Cl,OH)_4{\cdot}H_2O$, a new mineral species, and an associated lead-copper selenite chloride from the Baccu Locci mine, Sardinia, Italy. *Can. Mineral.* **1999**, *37*, 1493–1498.
17. Krivivichev, S.V.; Turner, R.; Rumsey, M.; Siidra, O.O.; Kirk, C.A. The crystal structure and chemistry of mereheadite. *Min. Mag.* **2009**, *73*, 103–117. [CrossRef]
18. Paar, W.H.; Braithwaite, R.S.W.; Chen, T.T.; Keller, P. A new mineral, scotlandite ($PbSO_3$) from Leadhills, Scotland: The first naturally occurring sulfite. *Min. Mag.* **1984**, *48*, 283–288. [CrossRef]
19. Grundmann, G.; Förster, H.-J. Origin of the El Dragón selenium mineralization, Quijarro province, Potosí, Bolivia. *Minerals* **2017**, *7*, 68. [CrossRef]
20. Keutsch, F.N.; Förster, H.-J.; Stanley, C.J.; Rhede, D. The discreditation of hastite, the orthorhombic dimorph of $CoSe_2$, and observations on trogtalite, cubic $CoSe_2$, from the type locality. *Can. Mineral.* **2009**, *47*, 969–976. [CrossRef]
21. Johan, Z.; Picot, P.; Kvačeck, M. La krut'aite, $CuSe_2$, un nouveau minéral du groupe da la pyrite. *Bull. Soc. Fr. Minéral. Cristallogr.* **1972**, *95*, 475–481.
22. Grundmann, G.; Lehrberger, G.; Schnorrer-Köhler, G. The El Dragón mine, Potosí, Bolivia. *Mineral. Rec.* **1990**, *21*, 133–146.
23. Bindi, L.; Cipriani, C.; Pratesi, G.; Trosti-Ferroni, R. The role of isomorphous substitutions in natural selenides belonging to the pyrite group. *J. Alloys Compd.* **2008**, *459*, 553–556. [CrossRef]
24. Criddle, A.J.; Stanley, C.J. *The Quantitative Data File for Ore Minerals*, 2nd ed.; British Museum (Natural History): London, UK, 1986; pp. 274–275.
25. Stanley, C.J.; Criddle, A.J.; Lloyd, D. Precious and base metal selenide mineralization at Hope's Nose, Torquay, Devon. *Mineral. Mag.* **1990**, *54*, 485–493. [CrossRef]
26. Diehl, S.F.; Goldhaber, M.B.; Koenig, A.E.; Lowers, H.A.; Ruppert, L.F. Distribution of arsenic, selenium, and other trace elements in high pyrite Appalachian coals; evidence for multiple episodes of pyrite formation. *Int. J. Coal Geol.* **2012**, *94*, 238–249. [CrossRef]
27. Parnell, J.; Brolly, C.; Spinks, S.; Bowden, S. Selenium enrichment in Carboniferous shales, Britain and Ireland: Problem or opportunity for shale gas extraction. *Appl. Geochem.* **2016**, *66*, 82–87. [CrossRef]
28. Yudovich, Y.E.; Ketris, M.P. Selenium in coal: A review. *Int. J. Coal Geol.* **2006**, *67*, 112–126. [CrossRef]
29. Krivovichev, V.; Charykova, M.; Vishnevsky, A. The thermodynamics of Se minerals in near-surface environment. *Minerals* **2017**, *7*, 188. [CrossRef]
30. Bullock, L.A.; Parnell, J.; Perez, M.; Feldmann, J.; Armstrong, J.G. Selenium and other trace element mobility in waste products and weathered sediments at Parysh Mountain copper mine, Anglesey, UK. *Minerals* **2017**, *7*, 229. [CrossRef]
31. Coleman, L.; Bragg, L.J.; Finkelman, R.B. Distribution and mode of occurrence of selenium in US coals. *Environ. Geochem. Health* **1993**, *15*, 215–227. [CrossRef] [PubMed]
32. Simon, G.; Kesler, S.E.; Essene, E.J. Phase relations among selenides, sulphides, tellurides, and oxides: II. Applications to selenide-bearing ore deposits. *Econ. Geol.* **1997**, *92*, 468–484. [CrossRef]